Nano Energy 110 (2023) 108392

Contents lists available at ScienceDirect

Nano Energy

journal homepage: www.elsevier.com/locate/nanoen

Self-powered angle-resolved triboelectric nanogenerator for underwater vibration localization

Jianchao Guo [a,b], Jiaqi He [a,b], Zuqing Yuan [a], Juan Tao [a], Xiangyu Liu [a,b], Zhuoyu Song [c], Wenchao Gao [a,b,*], Chunfeng Wang [d,**], Caofeng Pan [a,b,*]

[a] CAS Center for Excellence in Nanoscience, Beijing Key Laboratory of Micro-nano Energy and Sensor, Beijing Institute of Nanoenergy and Nanosystems, Chinese Academy of Sciences, Beijing 101400, PR China
[b] School of Nanoscience and Technology, University of Chinese Academy of Sciences, Beijing 100049, PR China
[c] Department of Engineering Mechanics, Dalian University of Technology, Dalian, Liaoning 116024, PR China
[d] College of Materials Science and Engineering, Guangdong Research Center for Interfacial Engineering of Functional Materials, Shenzhen University, Shenzhen 518060, PR China

ARTICLE INFO

Keywords:
Triboelectric nanogenerator
Self-powered
Angle-resolved
Underwater localization
Marine engineering

ABSTRACT

Precise locating in underwater environment is essential for marine engineering and national security. However, the current technologies usually suffer from energy and complexity issues. Here, a self-powered angle-resolved triboelectric nanogenerator (AR-TENG) is proposed for underwater vibration detecting and locating in a simple and energy-effective fashion. The AR-TENG is made of metal balls and an inverted conical unit consisting of fluorinated ethylene propylene film and multiple sector-like electrodes, where each electrode corresponding to one sensing channel. Each channel of AR-TENG can respond to low-frequency variations with linear electrical outputs and a maximum power density of 1.28 $\mu W \cdot cm^{-2}$ at a load resistance of 200 MΩ. Most importantly, the output voltage ratio of two adjacent channels is only related to the vibration direction, endowing AR-TENG with the capability of vibration direction recognition with an angle resolution of 15°. As a result, the underwater vibration locating can be realized by simply intersecting the vibration directions respectively determined by two AR-TENGs arranged in parallel, performing a locating accuracy of >95 %, assisted with a simple trigonometric function and geometric relation. This new scheme is simple, effective and energy-autonomous, holding great potential for various underwater applications.

1. Introduction

The internet of things in the context of the ocean has been emerging with the development of ocean exploration [1–3], wherein underwater localization technologies are expanded by leaps and bounds because almost all underwater applications depend deeply on location information [4–7]. The precise positioning technology represented by the Global Position System (GPS) is very mature and widely used in terrestrial scenarios. However, it loses efficacy in damp, dim and changeable underwater environment as GPS signals do not propagate through water [8,9]. The currently used methods for underwater localization mainly include sonar, optical positioning technologies, and electromagnetic positioning technologies [10–14]. Each of these methods has its problems, including but not limited to poor environmental friendliness, high system complexity, high energy consumption, short endurance, and high cost. Thus, the development of a fresh strategy to enable underwater detection and localization is highly desired.

Triboelectric nanogenerator (TENG) invented by Wang et al. in 2012 provides a novel paradigm for converting mechanical stimuli into electrical energy by utilizing the coupling effect of contact electrification and electrostatic induction [15–18]. With the merits of simple configuration, light weight, wide material choice, low cost and easy scalability [19–24], TENG has been applied to a myriad of fields, such as self-powered sensing and energy harvesting [25–32]. In particular, as a self-powered sensor, TENG can respond to vibration stimuli without any external power supply, promising underwater vibration detection and

* Corresponding authors at: CAS Center for Excellence in Nanoscience, Beijing Key Laboratory of Micro-nano Energy and Sensor, Beijing Institute of Nanoenergy and Nanosystems, Chinese Academy of Sciences, Beijing 101400, PR China.
** Corresponding author.
E-mail addresses: gaowenchao@binn.cas.cn (W. Gao), cfwang@szu.edu.cn (C. Wang), cfpan@binn.cas.cn (C. Pan).

https://doi.org/10.1016/j.nanoen.2023.108392
Received 28 February 2023; Received in revised form 19 March 2023; Accepted 26 March 2023
Available online 27 March 2023

localization in a simple and energy-autonomous way [33–35]. Accordingly, Yu et al. demonstrated a self-powered acoustic sensor based on organic film TENG to detect underwater targets at frequencies around 100 Hz [36]. Zhang et al. reported a cable-structured TENG network for underwater monitoring, assisted with a specially designed signal processing module [37]. Guan et al. presented an ultrasound-driven TENG (UD-TENG) for underwater ultrasonic wave detection and sound source localization [38]. Despite the thriving progress, the aforementioned devices suffer from weak stability aggravated by high frequency vibration, complicated calculation, and limited accuracy.

In this work, a self-powered angle-resolved triboelectric nanogenerator (AR-TENG) is designed for the convenient and precise detection and localization of underwater vibration. The AR-TENG consists of a number of metal balls and an inverted conical unit composed of fluorinated ethylene propylene (FEP) film and multiple sector-like electrodes, which are encapsulated in an acrylic ball. When stimulated by external vibration, the metal balls move on the sensing unit, causing electrical signals to be output. A maximum power density of 1.28 $\mu W \cdot cm^{-2}$ at a load resistance of 200 MΩ is obtained at low-frequency variations. The design of multiple sector-like electrodes endows the direction recognition capability of AR-TENG, exhibiting an angle-resolved resolution of 15°, which can be further improved at an expense of the signal-to-noise ratio. The location of the underwater vibration source can be simply determined by intersecting the vibration directions respectively detected by two AR-TENGs arranged in parallel, performing a relatively high accuracy rate of >95 % with the help of a simple trigonometric function and geometric relation.

2. Results and discussion

2.1. Design and operation of AR-TENG

The application perspectives of underwater localization realized by AR-TENGs are schematically shown in Fig. 1**a**. The sensor network

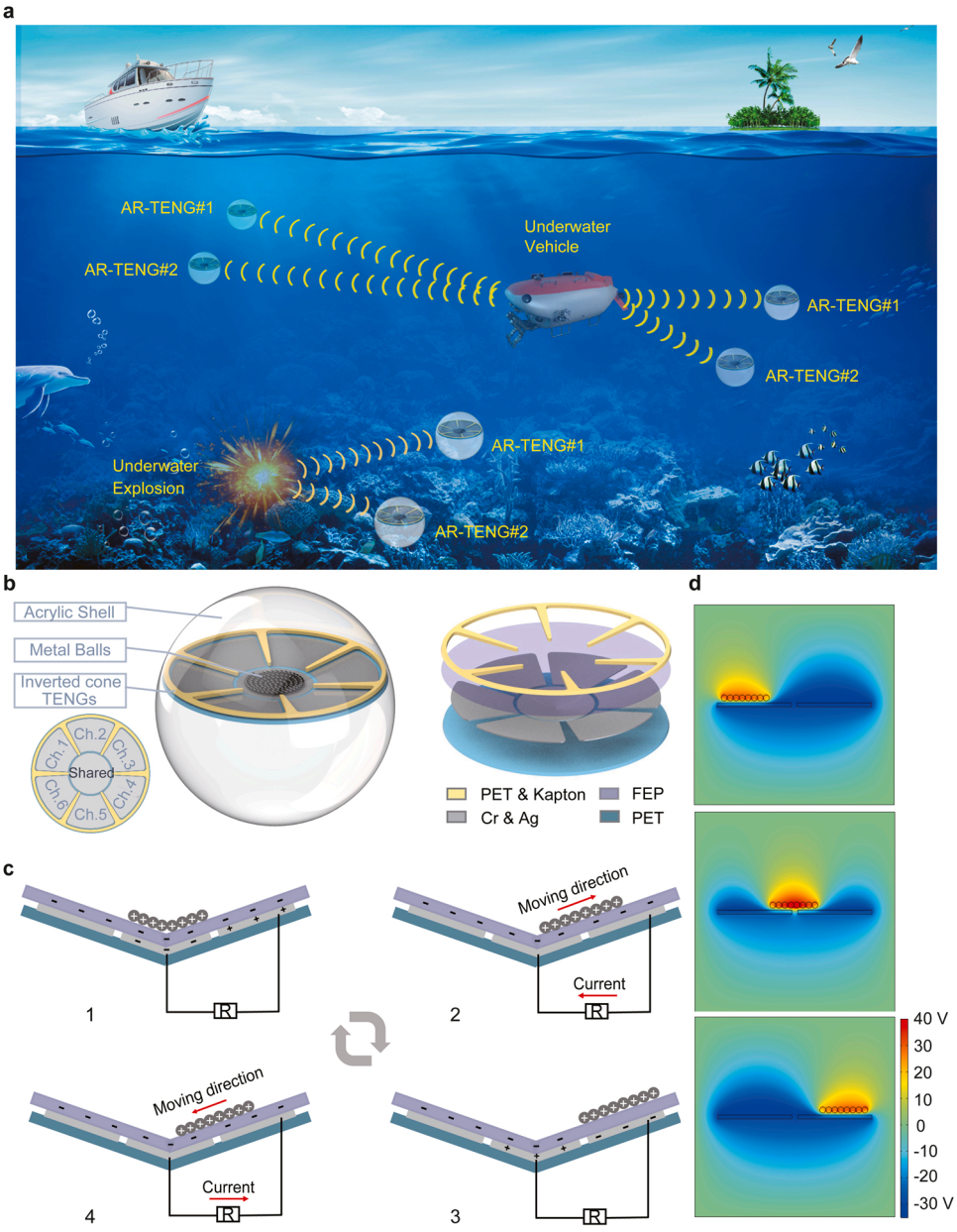

Fig. 1. Design and operation of AR-TENG. (a) Conceptual diagram of the AR-TENG for underwater detection and location. (b) Structure diagram of the AR-TENG. (c) The working principle of the AR-TENG and charge distribution in the workflow. (d) Simulation of the potential distribution of AR-TENG during normal operation.

contains pairs of AR-TENGs and is installed in the underwater environment. The vibrations caused by underwater vehicles, explosions and so on drive the AR-TENGs, which convert the vibrations into electrical signals. The electrical signals carry the location information of the vibration source, and accordingly, the location of the vibration source can be determined by data processing. Fig. 1**b** shows the structure diagram of one representative AR-TENG, consisting of numerous metal balls and an inverted conical unit composed of FEP film and multiple sector-like electrodes, integrated inside an acrylic ball. Polyethylene glycol terephthalate (PET) is chosen as the substrate that provides mechanical support to the unit owing to its good mechanical strength and flexibility [39,40]. The central circular electrode and the surrounding sector-like electrodes are made of Cr and Ag, where Cr acts as an adhesive layer [41]. The FEP film is used as the negative triboelectric layer due to its good electron affinity [27,42]. The customized barriers consisting of PET and Kapton are on the upper layer of FEP film, which can limit the chaotic motion of metal balls between the adjacent sensing channels. The fabrication process of AR-TENG is schematically shown in Fig. S1 and the specific parameters of every component are given in the Experimental Section.

The angle-resolved capability of AR-TENG is enabled by the multiple electrodes design, where each sector-like electrode corresponds to one sensing channel. Each sensing channel has a relatively good output uniformity (Fig. S2), and the serial numbers of each sensing channel are shown in the lower left panel of Fig. 1**b**. The channel number is optimized to be six, considering the balance between angle-resolved resolution and signal-to-noise ratio (SNR) defined by the output voltage ratio of two adjacent channels, as shown in Fig. S3-S4. The amount of metal balls is also a vital factor that affects the output performance of AR-TENG. Fig. S5 displays the performance comparison of AR-TENG with different amounts of metal balls. The results show that increasing metal balls could enhance the output voltage gradually. However, the SNR decreases dramatically when the metal balls exceed to a certain extent (180 balls) because the excessive metal balls would move disorderly among the sensing channels.

The working principle of AR-TENG is illustrated in Fig. 1**c**, where AR-TENG works under freestanding mode with FEP film acting as the freestanding layer. Briefly, the metal balls move on the FEP films upon vibration, resulting in the metal balls carrying positive charges while the FEP film becomes negatively charged due to their difference in electron affiliation, as shown in Fig. 1**c(i)**. As the surface charges are the trapped electrons in the potential well, they can maintain for a long time. With the positively charged metal balls moving from the central electrode to the right sector-like electrode, the negative charges are induced gradually on the right electrode. Due to the electrostatic potential, the flowing of electrons results in the current in the circuit, which has the opposite direction from the electron flowing, as shown in Fig. 1**c(ii)**. The current could exist until the metal balls reach the right sensing channel totally, as shown in Fig. 1**c(iii)**. When the metal balls move back from the right electrode to the central electrode, the direction of the electron flowing and the current in the circuit have the opposite direction compared with the former situation, as shown in Fig. 1**c(iv)**. With the back-and-forth motion of metal balls driven by the external vibration, the alternate current signal would be generated in the circuit. The COMSOL multiphysics software is used to stimulate the electrical potential distribution at each part of the moving process of the metal balls, as shown in Fig. 1**d**.

2.2. Performances of AR-TENG

The output performances of AR-TENG to vibration stimulation are systematically studied. In the measurement, AR-TENG is driven by a linear motor with different program parameters to simulate external vibrations (see Table S1 for program details). And only one sensing channel is tested and displayed because all six channels have the same structure and performance. The open-circuit voltages (V_{OC}) and short-circuit currents (I_{SC}) of AR-TENG as a function of vibration amplitudes are shown in Fig. 2**a** and **b**, respectively, where the vibration amplitudes change from 10 mm to 50 mm with an interval of 5 mm when the vibration frequency is kept at 1.5 Hz. Both V_{OC} and I_{SC} gradually increase as increasing the amplitudes owning to the sufficient motion of metal balls on FEP. However, the V_{OC} approaches to saturation when the amplitude exceeds 45 mm because the metal balls will move back and forth with no surplus charges transfer at a large vibration amplitude, as indicated by Fig. S6. Fig. 2**c** exhibits the fitting curves of V_{OC} and I_{SC} on vibration amplitudes ranging from 15 mm to 40 mm, showing an appropriate linear relationship. The dependence of V_{OC} and I_{SC} on vibration frequency is shown in Fig. 2**d** and **e**, respectively, where the vibration frequency varies from 1.2 Hz to 2 Hz while the vibration amplitude is fixed at 45 mm. It can be observed that the V_{OC} is almost constant at low-frequency vibration and decreases a little at relatively high-frequency vibration because the contact between metal balls and FEP film is not sufficient at relatively high vibration frequency. And the change of transfer charges shows similar characteristics to that of V_{OC}, as shown in Fig. S7. The I_{SC} increases monotonously with the increased vibration frequency because of the accelerated charges transfer at higher frequency, featuring a linear relationship (Fig. 2**f**).

The output voltages and currents of AR-TENG under different resistances are tested as well, as shown in Fig. 2**g**. The output voltages rise as the external load resistance increase, while the currents behave in the opposite trend. The power density of AR-TENG, $P_0 = (U \times I)/(R \times S)$, where U and I are the voltage and current under the external load resistance, R means the value of the external load resistance, S represents the area of the two sensing channels, reaches its peak value of 1.288 $\mu W \cdot cm^{-2}$ at a load resistance of 200 MΩ, as shown in Fig. 2**h**. Fig. 2**i** shows the response time of AR-TENG, with a value of around 180 ms. In addition, AR-TENG exhibits excellent stability, including long-term stability and cycling stability. Fig. 2**j** indicates that the V_{OC} only has a slight attenuation after 2 months, which is recorded every 10 days. And Fig. 2**k** shows that AR-TENG can work well after 10,000 cycles at a frequency of 1.5 Hz and an amplitude of 50 mm, guaranteeing AR-TENG for long-term and continuous applications.

2.3. AR-TENG for vibration direction recognition

The most important characteristic of the AR-TENG is that it responds differently to vibrations from different directions, which means AR-TENG has the capability of direction recognition. Here, the direction recognition test of AR-TENG is systematically studied. The device is attached to the linear motor using a special fixture, as shown in Fig. 3**a**. There are angle marks on the fixture, as shown in the inset of Fig. 3**a**, for the convenient determination of vibration directions, which is defined as the intersection angle between the direction of the linear motor motion and the central axis of the measured sector-like sensing channels, as shown in Fig. 3**b**, where the darkening channel is measured and a representative intersection angle of 30° is presented. We gradually increased the intersection angle from 0° to 360° with an interval of 15° and measured the output voltages and currents at a vibration frequency of 1.5 Hz and a vibration amplitude of 50 mm. The directional patterns of voltage and current are shown in Fig. 3**c** and **d**, respectively, exhibiting a similar trend as the intersection angle increases. In terms of voltage signals, the voltages at 0° and 180° directions reach the maximum values because the measured sensing channel is aligned with the vibration direction, in which the metal balls can almost completely move from the central circular electrode to the measured sector-like electrode. The minimum value of voltage appears at 90° and 270°, where the measured sensing channel is perpendicular to the vibration direction, with negligible metal balls passing through. Within each quarter, the voltage gradually increases or decreases as the intersection angle increases, depending on whether the measured sensing channel is approaching or deviating from the vibration direction.

As the AR-TENG has six centrosymmetric sensing channels with each channel occupied about 60°, there are always two opposite sensing

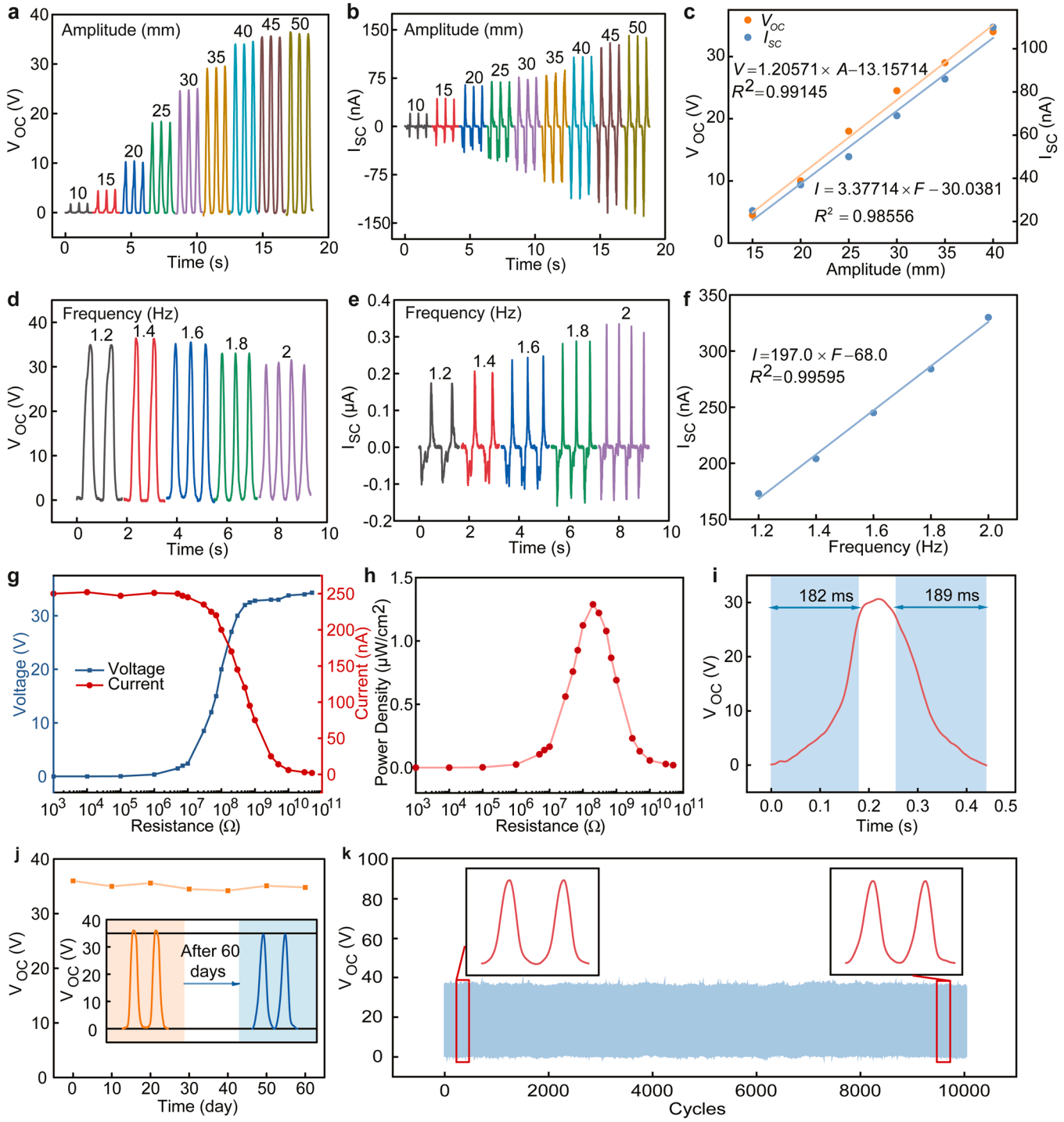

Fig. 2. Electrical performance of AR-TENG. (a,b) V_{oc} and I_{sc} of AR-TENG under different vibration amplitudes at a fixed vibration frequency of 1.5 Hz. (c) The fitted linear relationship of V_{oc} and I_{sc} on vibration amplitude. (d,e) V_{oc} and I_{sc} of AR-TENG under different vibration frequencies at a fixed vibration amplitude of 45 mm. (f) The fitted linear relationship between I_{sc} and vibration frequency. (g) The voltage and current outputs of AR-TENG with different external resistances. (h) Dependence of the power density of AR-TENG on different external resistances. (i) Response time of AR-TENG. (j) The durability of AR-TENG, with a stable V_{oc} output for 60 days. (k) Cyclic stability of AR-TENG, with a stable V_{oc} output for over 10,000 cycles.

channels roughly located in the vibration direction for every increase of 60° in the intersection angle. Thus, we only need to investigate the output signals from 0° to 60° for brevity. And the voltage signal is selected here due to its fewer influence factors than the current signal. As shown in Fig. 3**e**, the voltage has a linear dependence on the intersection angle ranging from 0° to 60°. However, the voltage signals will vary greatly with different vibration amplitudes at the same intersection angle, as shown in the solid line of Fig. 3**f**, indicating that it is not feasible to judge vibration direction only based on the voltage signal of one sensing channel because the voltage signals are affected by both vibration direction and vibration amplitude. Therefore, an output variable which only affected by vibration direction is needed. We measured the output voltages of the sensing channel adjacent to the previous one at different amplitudes and intersection angles, as shown in the dotted line of Fig. 3**f**. The adjacent sensing channel is at the intersection angle of 0° when the previous sensing channel is at 60° due to symmetry. We

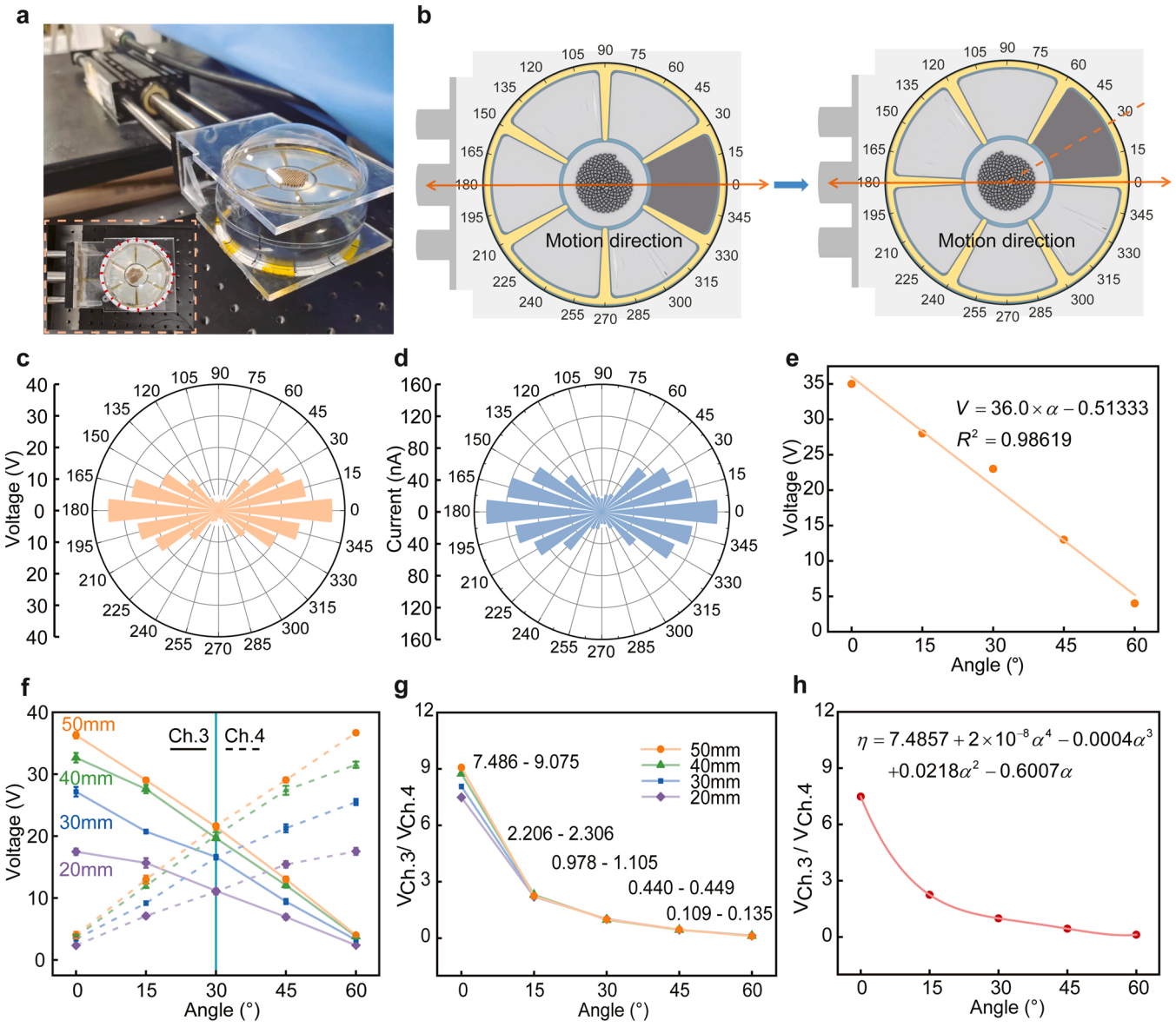

Fig. 3. AR-TENG for vibration direction recognition. (a) The setup of angle-resolved measurement. (b) Schematic illustration of the change of intersection angle. (c,d) The output patterns of voltage and current with different intersection angles. (e) The fitted linear relationship between the output voltage and the intersection angle. (f) The output voltages of two adjacent sensing channels at different vibration amplitudes and intersection angles. (g) The ratio of the output voltages of the two adjacent channels as a function of intersection angles at different vibration amplitudes. (h) The polynomial fitted line between the voltage ratio and the intersection angles.

calculate the ratio of the output voltages of the two channels corresponding to different intersection angles and display the result in Fig. 3**g**. It can be found that the ratio remains stable at different vibration amplitudes, offering an ideal variable for vibration direction recognition. Moreover, the ratio mentioned above is fitted by the polynomial, as shown in Fig. 3**h**, from which the vibration direction can be concretely determined by the conjunction of the measured voltages and the fitting result.

2.4. AR-TENG for underwater vibration localization

The localization of underwater vibration source can be conducted using a sensor array composed of two AR-TENGs arranged in parallel with a certain distance, where each AR-TENG can work independently to recognize the vibration direction. The intersection of two directions determined respectively by the two AR-TENGs gives the location information of the vibration source. The entire workflow is shown in Fig. 4**a**, which mainly includes four steps: 1) The sensor array detects vibration stimuli and generates corresponding electrical signals. 2) The electrical signals are collected using the test system composed of an electrometer and a computer server. 3) The vibration directions are obtained by analyzing the collected electrical signals assisted with the fitting line. 4) The vibration position is determined by intersecting the two vibration directions.

To verify this method, six different vibration positions are examined separately, and their coordinates are indicated in Fig. 4**b**. In addition, the output voltages of AR-TENG at difference distances away from the vibration source is also shown in Fig. S8. Taking position #1 (P1) as an example, the corresponding voltage pattern of AR-TENG#1 and AR-TENG#2 is shown in Fig. 4**c** and **d**, respectively, along with the dynamic distributions of metal balls upon vibrations simulated by the finite element analysis (see Experimental Section for details). The Ch.2 and Ch.5 of AR-TENG #1 generated much higher voltage than the other channels with almost the same output voltage, meaning that the

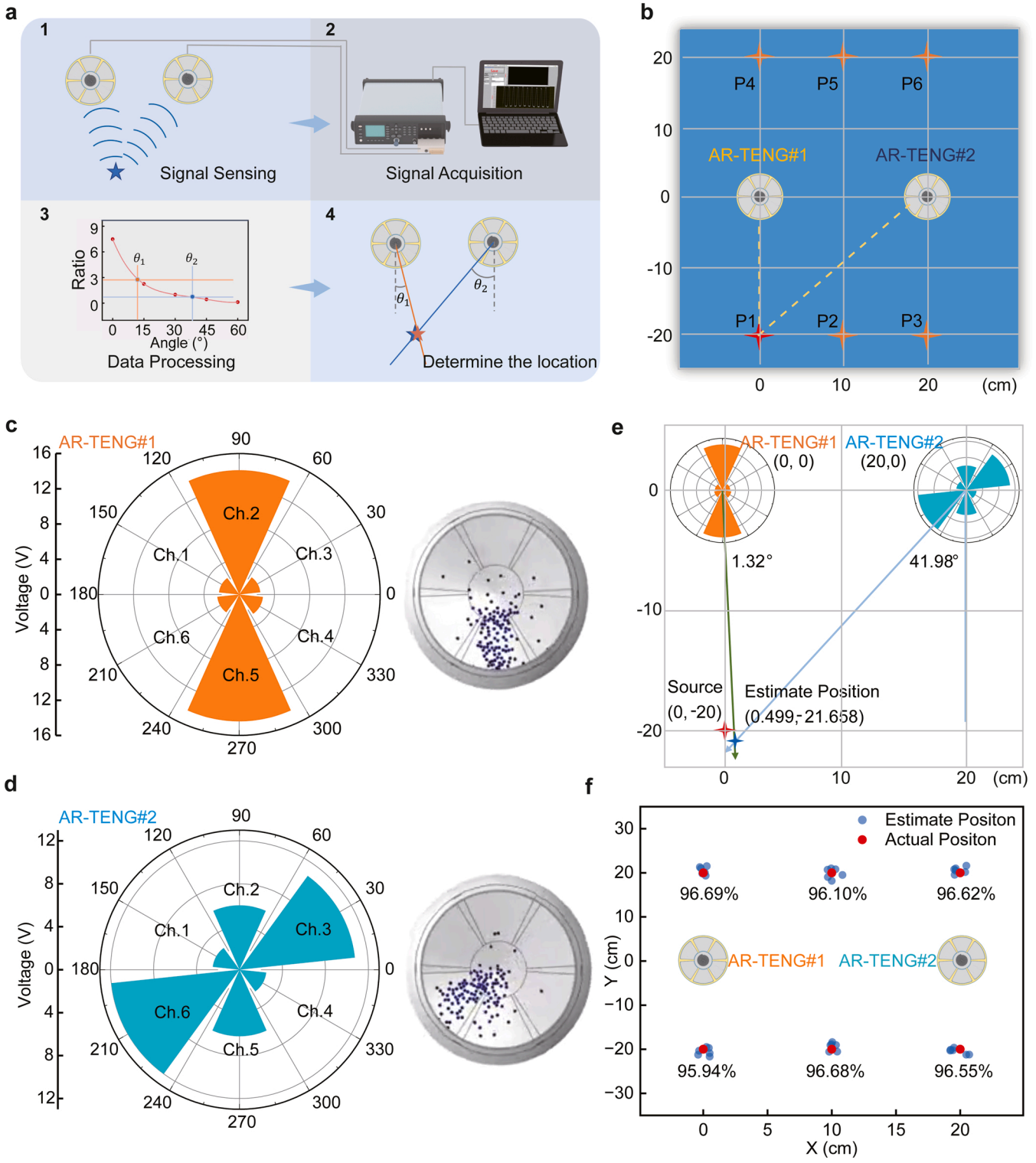

Fig. 4. AR-TENG for underwater vibration localization. (a) The workflow of underwater positioning using a sensor array consisting of two AR-TENGs. (b) The schematic of the vibration positions to be measured in the work. (c,d) The voltage pattern of AR-TENG#1 and AR-TENG#2, respectively, along with the dynamic distributions of metal balls upon vibrations simulated by the finite element analysis. (e) The location information of one representative vibration source calculated with the help of trigonometric function and geometric relation. (f) The statistics of localization accuracy from several vibration positions.

vibration direction is roughly along the central axis of Ch.2 and Ch.5. Nevertheless, the highest voltages appear in Ch.3 and Ch.6 for AR-TENG #2, followed by the relatively high voltages in Ch.2 and Ch.5 and the lowest voltages in Ch.1 and Ch.4. It means the vibration direction is between two sets of sensing channels, Ch.3, Ch.6 and Ch.2, Ch.5, and close to the central axis of Ch.3 and Ch.6. The voltage patterns and the corresponding dynamic distributions of metal balls for other positions are shown in Fig. S9 and **Video S1.** Afterward, the ratios of the voltage signals of two adjacent channels (Ch.5 and Ch.4 of AR-TENG #1, Ch.6 and Ch.5 of AR-TENG #2) are calculated and the vibration directions can be determined using the fitting line. And then the coordinate of the vibration source can be simply calculated with the help of trigonometric

function and geometric relation, as shown in Fig. 4**e**. The localization results and accuracy statistics of P1 to P6 are summarized in Fig. 4**f**, showing the locating accuracy is higher than 95 % for each position, indicating that this proposed approach is robust and precise.

Supplementary material related to this article can be found online at doi:10.1016/j.nanoen.2023.108392.

3. Conclusion

In summary, a self-powered and angle-resolved triboelectric nanogenerator is proposed and developed for underwater direction recognition and localization, exhibiting an angular resolution of 15° for direction recognition and a high accuracy of more than 95 % for localization. This proposed approach is simple, energy-efficient, robust and low-cost, promising their implementation in multitudinous underwater applications such as marine engineering and national security. Some further analysis of array integration and structural optimization will be studied in future work for higher angular recognition and extended applications.

4. Experimental section

4.1. Fabrication of AR-TENG

The PET film with a thickness of 100 μm was chosen to serve as the substrate of AR-TENG. A layer of Kapton tape was stuck on the cleaned PET substrate and then cut into the designed pattern by a lasing cutting system (Universal PLS6.75). The patterned electrode composed of 10 nm Cr and 100 nm Ag was deposited on the substrate using magnetron sputtering, followed by the peel-off of Kapton tape. The wires were led from each electrode and subsequently, a FEP film with a thickness of 40 μm was covered on the entire surface. Then, an inverted conical structure was constructed after cutting through the substrate along with the radius between two adjacent channel electrodes. A layer of customized barriers consisting of PET and Kapton was adhered to the FEP film at a position between adjacent electrodes to limit the chaotic motion of metal balls. The metal balls are made of brass, with a diameter of 1.588 mm and an average mass of 0.0179 g. Then, the aforementioned structure was integrated inside an acrylic ball, sealed by epoxy resin glue.

4.2. Characterizations

Electrical measurement of the TENG device: the linear motor (LinMot) was utilized to generate vibration. The electrical output (open-circuit voltage, the short-circuit current, the transferred charges, and the sensing electrical signals) of the device was measured by an electrometer (Keithley 6514), a low-noise current preamplifier (Stanford Research Systems SR570) and NI-DAQs (PCI-6259 and BNC-2110). The measuring program was built through LabView software.

4.3. FEA simulations

The simulation of the motion behavior of the sensor subjected to wave reaction was carried out in the commercial finite element software Abaqus 2019. The parts other than the metal sphere were suitably simplified considering the simulation purpose. Acrylic Shell and Inverted cone TENGs were modeled as shells and the R3D4 (four-node elements with bilinear quadrilateral) mesh was used; the metal spheres were modeled as solids and the C3D8R (eight-node brick elements with reduced integration and enhanced hourglass stiffness) mesh. An acceleration field was set in the Field module to simulate the gravitational force on the metal ball; a reference point was provided at the bottom of the sensor to control its motion, and a Periodic Amplitude was set in the Boundary module to simulate the sensor's response to signal sensing. The final solution was performed using Abaqus' dynamics (Explicit) solver.

CRediT authorship contribution statement

Jianchao Guo: Investigation, Conceptualization, Methodology, Data curation, Writing -original draft. **Jiaqi He:** Investigation, Writing - review & editing. **Zuqing Yuan:** Methodology, Writing - review & editing. **Juan Tao:** Writing - review & editing. **Xiangyu Liu:** Writing - review & editing. **Zhuoyu Song:** Visualization, Writing - review & editing. **Wenchao Gao:** Simulation, Visualization, Supervision, Writing - review & editing. **Chunfeng Wang:** Investigation, Methodology, Supervision, Writing - review & editing. **Caofeng Pan:** Methodology, Data curation, Supervision, Validation, Writing - review & editing.

Declaration of Competing Interest

The authors declare that they have no known competing financial interests or personal relationships that could have appeared to influence the work reported in this paper.

Data availability

Data will be made available on request.

Acknowledgments

This work was supported by the National Natural Science Foundation of China (52125205, U20A20166, U22A2077, 52192614 and 52002246), the Shenzhen Fundamental Research Project (JCYJ20190808170601664), the Shenzhen Science and Technology Program (KQTD20170810105439418), the Science and Technology Innovation Project of Shenzhen Excellent Talents (RCBS20200714114919006), National key R&D program of China (2021YFB3200302 and 2021YFB3200304), and the Fundamental Research Funds for the Central Universities.

Appendix A. Supporting information

Supplementary data associated with this article can be found in the online version at doi:10.1016/j.nanoen.2023.108392.

References

[1] V. Marx, The big challenges of big data, Nature 498 (2013) 255–260.
[2] R. Haight, W. Haensch, D. Friedman, Solar-powering the internet of things, Science 353 (2016) 124–125.
[3] K.Q. Wang, W.H. Xu, W. Zhang, X. Wang, X. Yang, J.F. Li, H.L. Zhang, J.J. Li, Z. K. Wang, Bio-inspired water-driven electricity generators: From fundamental mechanisms to practical applications, Nano Res. Energy 2 (2022), e912004.
[4] R.C. Shit, S. Sharma, D. Puthal, A.Y. Zomaya, Location of things (lot): a review and taxonomy of sensors localization in iot infrastructure, IEEE Commun. Surv. Tut. 20 (2018) 2028–2061.
[5] C. Hou, G.A. Tai, Y. Liu, Z.T. Wu, X.C. Liang, X. Liu, Borophene-based materials for energy, sensors and information storage applications, Nano Res. Energy 2 (2023), e912005.
[6] Y.F. Hu, J. Yang, Q.S. Jing, S.M. Niu, W.Z. Wu, Z.L. Wang, Triboelectric nanogenerator built on suspended 3d spiral structure as vibration and positioning sensor and wave energy harvester, ACS Nano 7 (2013) 10424–10432.
[7] W. Yan, G. Noel, G. Loke, E. Meiklejohn, T. Khudiyev, J. Marion, G.C. Rui, J.N. Lin, J. Cherston, A. Sahasrabudhe, J. Wilbert, I. Wicaksono, R.W. Hoyt, A. Missakian, L. Zhu, C. Ma, J. Joannopoulos, Y. Fink, Single fibre enables acoustic fabrics via nanometre-scale vibrations, Nature 603 (2022) 616–623.
[8] K.J. Ma, H.Y. Chen, Z.J. Wu, X.L. Hao, G. Yan, W.B. Li, L. Shao, G. Meng, W. M. Zhang, A wave-confining metasphere beamforming acoustic sensor for superior human-machine voice interaction, Sci. Adv. 8 (2022) eadc9230.
[9] P. Xu, J.H. Liu, X.Y. Liu, X.Y. Wang, J.X. Zheng, S.Y. Wang, T.Y. Chen, H. Wang, C. Wang, X.P. Fu, G.M. Xie, J. Tao, M.Y. Xu, A bio-inspired and self-powered triboelectric tactile sensor for underwater vehicle perception, Npj Flex. Electron 6 (2022) 25.
[10] H. Joe, H. Cho, M. Sung, J. Kim, S.C. Yu, Sensor fusion of two sonar devices for underwater 3d mapping with an auv, Auton. Robot. 45 (2021) 543–560.

[11] W.Y. Chen, Z. Liu, H.W. Zhang, M.Y. Chen, Y.P. Zhang, A submarine pipeline segmentation method for noisy forward-looking sonar images using global information and coarse segmentation, Appl. Ocean. Res. 112 (2021), 102691.
[12] F. Eren, S. Pe'eri, M.W. Thein, Y. Rzhanov, B. Celikkol, M.R. Swift, Position, orientation and velocity detection of unmanned underwater vehicles (uuvs) using an optical detector array, Sensors 17 (2017) 1741.
[13] T. Zhang, J. Yang, L. Guo, P.W. Hu, X. Liu, P.P. Huang, C.L. Wang, A bionic point-source polarisation sensor applied to underwater orientation, J. Navig. 74 (2021) 1057–1072.
[14] Q. Zhang, Y. Wang, D.S. Li, J. Xie, K. Tao, P.A. Hu, J. Zhou, H.L. Chang, Y.Q. Fu, Multifunctional and wearable patches based on flexible piezoelectric acoustics for integrated sensing, localization, and underwater communication, Adv. Funct. Mater. 33 (2023), 2209667.
[15] F.R. Fan, Z.Q. Tian, Z.L. Wang, Flexible triboelectric generator, Nano Energy 1 (2012) 328–334.
[16] Z.L. Wang, On maxwell's displacement current for energy and sensors: the origin of nanogenerators, Mater. Today 20 (2017) 74–82.
[17] Z.Q. Yuan, C.F. Pan, Quantifying electron-transfer in liquid-solid contact electrification, Sci. Bull. 65 (2020) 868–869.
[18] Q.X. Zeng, A. Chen, X.F. Zhang, Y.L. Luo, L.M. Tan, X. Wang, A dual-functional triboelectric nanogenerator based on the comprehensive integration and synergetic utilization of triboelectrification, electrostatic induction, and electrostatic discharge to achieve alternating current/direct current convertible outputs, Adv. Mater. 35 (2023), 2208139.
[19] F. Shen, Z.J. Li, H.Y. Guo, Z.B. Yang, H. Wu, M. Wang, J. Luo, S.R. Xie, Y. Peng, H. Y. Pu, Recent advances towards ocean energy harvesting and self-powered applications based on triboelectric nanogenerators, Adv. Electron. Mater. 7 (2021), 2100277.
[20] J.X. Zhu, M.L. Zhu, Q.F. Shi, F. Wen, L. Liu, B.W. Dong, A. Haroun, Y.Q. Yang, P. Vachon, X.G. Guo, T.Y.Y. He, C.K. Lee, Progress in teng technology-a journey from energy harvesting to nanoenergy and nanosystem, EcoMat 2 (2020), e12058.
[21] H.F. Zhao, M.Y. Xu, M.R. Shu, J. An, W.B. Ding, X.Y. Liu, S.Y. Wang, C. Zhao, H. Y. Yu, H. Wang, C. Wang, X.P. Fu, X.X. Pan, G.M. Xie, Z.L. Wang, Underwater wireless communication via teng-generated maxwell's displacement current, Nat. Commun. 13 (2022) 3325.
[22] Z.L. Wang, T. Jiang, L. Xu, Toward the blue energy dream by triboelectric nanogenerator networks, Nano Energy 39 (2017) 9–23.
[23] Z.L. Wang, Nanogenerators, self-powered systems, blue energy, piezotronics and piezo-phototronics - a recall on the original thoughts for coining these fields, Nano Energy 54 (2018) 477–483.
[24] J. Wu, W.L. Liu, Q.X. Zeng, Y. Zhang, H.Y. Guo, X.F. Zhang, W.C. He, Y.L. Luo, X. Wang, Z.L. Wang, A mutual boosting self-excitation hybrid cell for harvesting high entropy energy at 32% efficiency, Small 18 (2022), 2205704.
[25] Z.W. Ren, X. Liang, D. Liu, X.J. Li, J.F. Ping, Z.M. Wang, Z.L. Wang, Water-wave driven route avoidance warning system for wireless ocean navigation, Adv. Energy Mater. 11 (2021), 2101116.
[26] H.Y. Xu, J. Tao, Y. Liu, Y.P. Mo, R.R. Bao, C.F. Pan, Fully fibrous large-area tailorable triboelectric nanogenerator based on solution blow spinning technology for energy harvesting and self-powered sensing, Small 18 (2022), 2202477.
[27] Z.Q. Yuan, C.F. Wang, J.G. Xi, X. Han, J. Li, S.T. Han, W.C. Gao, C.F. Pan, Spherical triboelectric nanogenerator with dense point contacts for harvesting multidirectional water wave and vibration energy, ACS Energy Lett. 6 (2021) 2809–2816.
[28] X. Hang, T. Jiang, G.X. Liu, T.X. Xiao, L. Xu, W. Li, F.B. Xi, C. Zhang, Z.L. Wang, Triboelectric nanogenerator networks integrated with power management module for water wave energy harvesting, Adv. Funct. Mater. 29 (2019), 1807241.
[29] X.Y. Li, J. Tao, X.D. Wang, J. Zhu, C.F. Pan, Z.L. Wang, Networks of high performance triboelectric nanogenerators based on liquid-solid interface contact electrification for harvesting low-frequency blue energy, Adv. Energy Mater. 8 (2018), 1800705.
[30] J. An, Z.M. Wang, T. Jiang, X. Liang, Z.L. Wang, Whirling-folded triboelectric nanogenerator with high average power for water wave energy harvesting, Adv. Funct. Mater. 29 (2019), 1904867.
[31] Y.X. Hu, X.Y. Li, Z.H. Zhao, C.G. Zhang, L.L. Zhou, Y.H. Li, Y.B. Liu, J. Wang, Z. L. Wang, Triboelectric nanogenerator with low crest factor via precise phase difference design realized by 3d printing, Small Methods 5 (2021), 2100936.
[32] D.J. Tan, Q.X. Zeng, X. Wang, S.L. Yuan, Y.L. Luo, X.F. Zhang, L.M. Tan, C.G. Hu, G. L. Liu, Anti-overturning fully symmetrical triboelectric nanogenerator based on an elliptic cylindrical structure for all-weather blue energy harvesting, Nano-Micro Lett. 14 (2022) 124.
[33] J. Tao, R.R. Bao, X.D. Wang, Y.Y. Peng, J. Li, S. Fu, C.F. Pan, Z.L. Wang, Self-powered tactile sensor array systems based on the triboelectric effect, Adv. Funct. Mater. 29 (2019), 1806379.
[34] W.L. Wang, J.B. Pang, J. Su, F.J. Li, Q. Li, X.X. Wang, J.G. Wang, B. Ibarlucea, X. Y. Liu, Y.F. Li, W.J. Zhou, K. Wang, Q.F. Han, L. Liu, R.H. Zang, M.H. Rummeli, Y. Li, H. Liu, H. Hu, G. Cuniberti, Applications of nanogenerators for biomedical engineering and healthcare systems, InfoMat 4 (2022), e12262.
[35] C.S. Wu, A.C. Wang, W.B. Ding, H.Y. Guo, Z.L. Wang, Triboelectric nanogenerator: a foundation of the energy for the new era, Adv. Energy Mater. 9 (2019), 1802906.
[36] A.F. Yu, M. Song, Y. Zhang, Y. Zhang, L.B. Chen, J.Y. Zhai, Z.L. Wang, Self-powered acoustic source locator in underwater environment based on organic film triboelectric nano-generator, Nano Res 8 (2015) 765–773.
[37] Y.H. Zhang, Y.Y. Li, R.W. Cheng, S. Shen, J. Yi, X. Peng, C. Ning, K. Dong, Z. L. Wang, Underwater monitoring networks based on cable-structured triboelectric nanogenerators, Research 2022 (2022), 9809406.
[38] Z.X. Guan, L.Q. Liu, X.Y. Xu, A.C. Liu, H. Wu, J. Li, O.Y. Wei, A self-powered acoustic sensor excited by ultrasonic wave for detecting and locating underwater ultrasonic sources, Nano Energy 104 (2022), 107879.
[39] W.H. Xu, H.X. Zheng, Y. Liu, X.F. Zhou, C. Zhang, Y.X. Song, X. Deng, M. Leung, Z. B. Yang, R.X. Xu, Z.L. Wang, X.C. Zeng, Z.K. Wang, A droplet-based electricity generator with high instantaneous power density, Nature 578 (2020) 392–396.
[40] Y. Liu, R.R. Bao, J. Tao, J. Li, M. Dong, C.F. Pan, Recent progress in tactile sensors and their applications in intelligent systems, Sci. Bull. 65 (2020) 70–88.
[41] Y.X. Wan, J. Tao, M. Dong, L. Zhang, Z.C. Peng, R.R. Bao, C.F. Pan, Flexible intelligent sensing system for plane complex strain monitoring, Adv. Mater. Technol. 7 (2022), 2200386.
[42] Q. Jiang, B. Chen, Y. Yang, Wind-driven triboelectric nanogenerators for scavenging biomechanical energy, ACS Appl. Energy Mater. 1 (2018) 4269–4276.

Jianchao Guo received his B.S. degree in physics from Beijing Normal University in 2020. He is currently a Master student in the research group of Prof. Caofeng Pan at Beijing Institute of Nanoenergy and Nanosystems, Chinese Academy of Sciences. His research interests mainly focus on self-powered sensors and systems.

Jiaqi He received his B.S. degree in materials science and engineering from Southwest Jiaotong University in 2019. He is currently pursuing his PhD degree in the School of Nanoscience and Technology at University of Chinese Academy of Sciences under the supervision of Prof. Caofeng Pan. His current research is focused on flexible luminescent materials and optoelectronic memory devices.

Zuqing Yuan received his B.S. degree in materials science and engineering from University of Science and Technology Beijing in 2014. And then he earned his Ph.D. degree from Beijing Institute of Nanoenergy and Nanosystems, Chinese Academy of Sciences in 2019. His main research interests focus on the nanomaterials, polymer-based energy harvesting and smart device for flexible electronics.

Juan Tao received her B.S. degree in materials science and engineering from China University of Geosciences Beijing in 2015, and her Ph.D. degree in Institude of Semiconductors, Chinese Academy of Sciences in 2020. Her research interests mainly focus on flexible tactile sensors.

Xiangyu Liu received his B.S. degree (2020) in materials science and engineering from the Tsinghua University, China. He is currently a Master student in the research group of Prof. Caofeng Pan at Beijing Institute of Nanoenergy and Nanosystems, Chinese Academy of Sciences. His research interests mainly focus on field effect transistors based on two dimensional materials.

Zhuoyu Song received his B.S. degree in engineering mechanics from China University of Petroleum in 2019, and now is pursuing his Ph.D. degree at Dalian University of Technology. His research interests mainly focus on behavior prediction of the thermoplastic fiber reinforced composites, structural optimization and lightweight design.

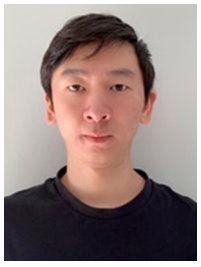

Prof. Wenchao Gao received Ph.D. from the Monash University in 2020. He is currently a professor and a group leader at Beijing Institute of Nanoenergy and Nanosystems, Chinese Academy of Sciences. He has worked for more than 5 years in the areas of nanomaterials design/characterization, multi-scale coupled numerical modelling and experimental validation on electrohydrodynamic, corona discharge, particle charging and particle trajectories, and mechanics of structures.

Prof. Chunfeng Wang received his B.S. degree in materials science and engineering from Zhengzhou University in 2013, and his Ph.D. degree in materials processing engineering from Zhengzhou University in 2019. He is currently an assistant professor in College of Materials Science and Engineering, Shenzhen University. His research interests include optoelectronic materials and soft devices.

Prof. Caofeng Pan received his B.S. degree (2005) and Ph.D. degree (2010) in materials science and engineering from the Tsinghua University, China. He is currently a professor and a group leader at the Beijing Institute of Nanoenergy and Nanosystems, Chinese Academy of Sciences. His research interests mainly focus on the fields of piezotronics/piezophototronics for fabricating new electronic and optoelectronic devices, nanopower source, hybrid nanogenerators, and self-powered nanosystems.